Metal Ion Stabilization of the U-Turn of the A_{37} N^6-Dimethylallyl-Modified Anticodon Stem−Loop of *Escherichia coli* $tRNA^{Phe}$†

Javier Cabello-Villegas,‡ Izabela Tworowska, and Edward P. Nikonowicz*

Department of Biochemistry and Cell Biology, Rice University, Houston, Texas 77251-1892

Received August 1, 2003; Revised Manuscript Received November 10, 2003

ABSTRACT: Nucleoside base modifications can alter the structures, dynamics, and metal ion binding properties of transfer RNA molecules and are important for accurate aminoacylation and for maintaining translational fidelity and efficiency. The unmodified anticodon stem−loop from *Escherichia coli* $tRNA^{Phe}$ forms a trinucleotide loop in solution, but Mg^{2+} and dimethylallyl modification of A_{37} N6 disrupt the loop conformation and increase the mobility of the loop and loop-proximal nucleotides. We have used NMR spectroscopy to investigate the binding and structural effects of multivalent cations on the unmodified and dimethylallyl-modified anticodon stem−loops from *E. coli* $tRNA^{Phe}$. The divalent cation binding sites were probed using Mn^{2+} and $Co(NH_3)_6^{3+}$. These ions bind along the major groove of the stem and associate with the anticodon loop on the major groove side in a nonspecific manner. $Co(NH_3)_6^{3+}$ stabilizes the U-turn conformation of the loop in the dimethylallyl-modified molecule, and the chemical shift changes that accompany $Co(NH_3)_6^{3+}$ binding are similar to those observed with the addition of Mg^{2+}. The base−phosphate and base−2′-OH hydrogen bonds that characterize the UNR U-turn motif lead to spectral signatures in the form of unusual ^{15}N and ^1H chemical shifts and reduced solvent exchange of the U_{33} 2′-OH and N3H protons. The unmodified molecule also displays spectral features of the U-turn fold in the presence of $Co(NH_3)_6^{3+}$, but the loop has additional conformations and is dynamic. The results indicate that charge neutralization by a polyvalent cation is sufficient to promote formation of the U-turn fold. However, base modification is necessary to destabilize competing alternative conformers even for a purine-rich loop sequence that is predicted to have strongly favorable base stacking energy.

The U-turn is an RNA structural motif that was first identified in the anticodon stem−loop of crystalline yeast $tRNA^{Phe}$ and is now recognized as a basic architectural unit of many RNA molecules. The U-turn reverses the direction of the phosphate backbone, frequently 3′ to a uridine nucleotide. The turn is achieved by adoption of the non-standard *trans* conformation of the α torsion angle 3′ to the uridine and is often stabilized by hydrogen bond and stacking interactions (*1*, *2*). The U-turn also has been identified in the solution structures of RNAs including tetraloops of the GNRA class (*3*), a conserved UGAA tetraloop found in 18S eukaryotic rRNA (*4*), the HIV-1 A-rich loop (*5*), the hammerhead ribozyme (*6*), and a conserved hexanucleotide loop found in 23S ribosomal RNA (*7*, *8*). Interestingly, the unmodified anticodon stem−loops from initiator and elongator $tRNA^{Met}$ form U-turns in solution (*9*), but the anticodon stem−loops of human $tRNA^{Lys,3}$ and *Escherichia coli* $tRNA^{Phe}$ do not (*10*, *11*).

Metal ions play important roles in the structures and catalytic functions of RNA molecules. These cations assist RNA folding and stabilize RNA tertiary structures by balancing local electrostatic environments. The tertiary structure of yeast $tRNA^{Phe}$ is stabilized by Mg^{2+} ions that tightly bind at four sites (*12*, *13*). In addition to these sites, crystallographic studies of yeast $tRNA^{Phe}$ reveal positions that bind Mg^{2+} less tightly, including within the anticodon stem−loop (*14*). Solution NMR[1] studies also support the presence of low-affinity or nonspecific binding sites for Mg^{2+} ions in the anticodon region (*15*).

Nucleotide base modification can alter the structure, stability, and metal ion affinity of RNA molecules (reviewed in ref *16*). Threonyl modification of A_{37} of $tRNA^{Lys,3}$ disrupts the hydrogen bond network of the loop, and hypermodification within the anticodon stem−loop promotes and stabilizes the U-turn fold (*17*, *18*). In *E. coli* $tRNA^{Val}$, Mg^{2+} stabilizes secondary structure, and tertiary interactions and modification increase the affinity of Mg^{2+} binding sites within the D stem and the anticodon stem−loop (*19*). In mature *E. coli* $tRNA^{Phe}$, A_{37} is replaced by $ms^2i^6A_{37}$. The modification enzyme dimethylallyl (Δ^2-isopentenyl) diphosphate:tRNA transferase (MiaA) catalyzes the addition of the dimethylallyl unit from dimethylallyl diphosphate (DMAPP) to produce the N^6-isopentenyl-modified A_{37}, i^6A_{37}. This modification occurs in 10 of 46 *E. coli* tRNA species and

† This work was supported by NSF Grant MCB-0078501 and by a grant from the Robert A. Welch Foundation (C1277) to E.P.N.

* Address correspondence to this author. Telephone: (713) 348-4912. Fax: (713) 348-5154. E-mail: edn@bioc.rice.edu.

‡ Present address: National Cancer Institute, Frederick, MD.

[1] Abbreviations: $ACSL^{Phe}$, anticodon stem−loop of *Escherichia coli* $tRNA^{Phe}$ (GAA); i^6A_{37} $ACSL^{Phe}$, A_{37} N^6-dimethylallyl-modified anticodon stem−loop of *E. coli* $tRNA^{Phe}$ (GAA); NTP, nucleoside triphosphate; NMR, nuclear magnetic resonance; NOE, nuclear Overhauser effect; NOESY, NOE spectroscopy; 2D, two dimensional; 3D, three dimensional; HetCor, heteronuclear correlation; HMQC, heteronuclear multiple-quantum coherence; HSQC, heteronuclear single-quantum coherence; NH, imino; NH_2, amino.

10.1021/bi0353676 CCC: $27.50
Published on Web 12/11/2003

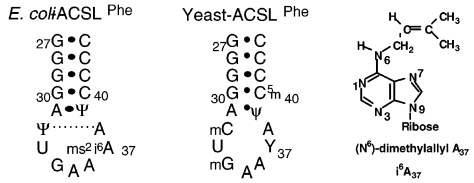

FIGURE 1: Nucleotide sequences corresponding to fully modified anticodon arms of *E. coli* $tRNA^{Phe}$ and yeast $tRNA^{Phe}$. Nucleotide numbering corresponds to the full-length tRNA molecule. The unmodified *E. coli* $tRNA^{Phe}$ forms a triloop with base pairs U_{32}•A_{38} and U_{33}•A_{37}. The i^6A_{37} $ACSL^{Phe}$ molecule contains only the dimethylallyl modification at A_{37} (right).

disrupts intraloop hydrogen bonds in *E. coli* $tRNA^{Phe}$ due to steric clashes (*11*).

We have used heteronuclear NMR spectroscopy to probe the metal ion binding sites and examine the structural effects of metal ion binding on the unmodified and MiaA-modified forms of the anticodon arm of *E. coli* $tRNA^{Phe}$. These studies were conducted using a 17-nucleotide RNA molecule that forms a stem−loop secondary structure in solution (Figure 1). Our results demonstrate that the anticodon loop can adopt multiple conformations in the presence of multivalent cations and that cobalt hexamine more effectively stabilizes these conformations than Mg^{2+}. The data also show that the dimethylallyl modification alters the relative stabilities of the metal ion-induced conformers so that only the U-turn fold of the loop is observed in the presence of cobalt hexamine. The dimethylallyl modification may destabilize otherwise energetically favorable metal ion-induced conformations of the anticodon loop that compete with the U-turn fold.

MATERIALS AND METHODS

All enzymes were purchased from Sigma Chemical Co., except for the T7 RNA polymerase and dimethylallyl diphosphate:tRNA prenyl transferase enzymes, which were prepared as described (*20*, *21*). Deoxyribonuclease I type II, pyruvate kinase, adenylate kinase, and nucleotide monophosphate kinase were obtained as powders, dissolved in 15% glycerol, 1 mM dithiothreitol, and 10 mM Tris-HCl, pH 7.4, and stored at −20 °C. Guanylate kinase and nuclease P1 were obtained as solutions and stored at −20 °C. Unlabeled 5′-nucleoside triphosphates (5′-NTPs) were purchased from Sigma, phosphoenolpyruvate (potassium salt) was purchased from Bachem, and 99% [^{15}N]ammonium sulfate and 99% [^{13}C]methanol were purchased from Cambridge Isotope Laboratories. γ,γ-Dimethylallyl diphosphate (DMAPP) was purchased from Sigma.

Preparation of RNA Samples. The RNA sequence for *E. coli* $ACSL^{Phe}$ shown in Figure 1 was synthesized in vitro using T7 RNA polymerase and a synthetic DNA template. The nucleotide sequence of the stem corresponds to residues G_{27}−C_{43} of full-length *E. coli* $tRNA^{Phe}$. Isotopically labeled RNA molecules were prepared from 10 mL transcription reactions using 3 mM uniformly ^{15}N-enriched and ^{13}C-enriched 5′-NTPs as described (*22*). The RNA molecules were purified by passage through 20% (w/v) preparative polyacrylamide gels, electroeluted (Schleicher & Schuell), and precipitated with ethanol. The purified oligonucleotides were dissolved in 1.0 M NaCl, 20 mM potassium phosphate, pH 6.8, and 2.0 mM EDTA and dialyzed extensively against 10 mM NaCl, 10 mM potassium phosphate, pH 6.8, and 0.05 mM EDTA (low salt buffer). The samples were diluted with low salt buffer to a volume of 200 μL and lyophilized to a powder. For experiments involving the nonexchangeable protons, the samples were exchanged once with 99.96% D_2O and then resuspended in 200 μL of 99.96% D_2O. For experiments involving detection of the exchangeable protons, the samples were resuspended in 200 μL of 90% H_2O/10% D_2O. The samples contained 50−130 A_{260} OD units of unmodified RNA oligonucleotide in 200 μL (≈1.7−4.3 mM) and 75−100 A_{260} OD units of modified RNA oligonucleotide (≈2.5−3.4 mM).

Preparation of the A_{37} N^6-Dimethylallyl-Modified $ACSL^{Phe}$. The dimethylallyl modification was introduced at position A_{37} of purified $ACSL^{Phe}$ using the enzyme MiaA dimethylallyl diphosphate:tRNA transferase and DMAPP (*11*). Histidine-tagged MiaA was expressed in *E. coli* and purified using Ni^{2+} affinity resin as described (*20*). The typical modification reaction was performed using 50 μM $ACSL^{Phe}$, 125 μM DMAPP, 50 mM Tris-HCl, pH 7.6, 10 mM $MgCl_2$, 0.1 mg/mL BSA, 5 mM β-mercaptoethanol, and 26 μg/mL MiaA. The reactions were incubated overnight at 30 °C. Upon completion, the solution was extracted with cold phenol−chloroform−isoamyl alcohol (25:24:1) and chloroform, and the RNA was precipitated with ethanol. The reactions were monitored using 20% denaturing PAGE and proceeded to ≥95% completion. The modified $ACSL^{Phe}$ migrates slower than unmodified $ACSL^{Phe}$ and leads to a band shift equivalent to one additional nucleotide.

NMR Spectroscopy. All NMR spectra were acquired on a Bruker AMX-500 spectrometer equipped with a ^{1}H−{X} broad-band probe. Broad-band decoupling of the carbon and nitrogen resonances was achieved using GARP with γB_2 = 3125 Hz for carbon and γB_2 = 1570 Hz for nitrogen. H_2O spectra were collected at 12 °C with solvent suppression using either spin lock pulses or binomial $1\bar{1}$ or $1\bar{3}\ 3\bar{1}$ read pulses. D_2O spectra were collected at 25 °C with presaturation or spin lock pulses to suppress the residual HDO peak. Quadrature detection was achieved using the States−TPPI method, and acquisition was delayed by a half-dwell in all indirectly detected dimensions. Typically, the data points were extended by 25% using linear prediction for the indirectly detected dimensions, and the data were apodized using 1 Hz line broadening and 65 deg shifted sine-bell functions. ^{1}H spectra were referenced to DSS (0.00 ppm). References for the ^{13}C and ^{15}N spectra were calculated using the spectrometer frequencies. The ^{31}P spectra were referenced to an external standard of TMP which was set at 0.00 ppm. All spectra were processed and analyzed with Felix 98.0 (Molecular Simulations, Inc.).

Base and ribose resonances were sequentially correlated using NOESY and multiple-bond ^{15}N−^{1}H HSQC experiments. The adenine C2−H2 pairs were correlated to the C8−H8 pairs of the same base using an HCCH-TOCSY spectrum, and the 2′ chemical shifts were assigned by correlation to the H1′ resonances using an HCCH-COSY spectrum.

Distance constraints for the nonexchangeable resonances of modified $ACSL^{Phe}$ were derived at 25 °C from 2D ^{1}H−^{1}H NOESY spectra (180 and 360 ms mixing times). Similar experiments were acquired for the nonexchangeable resonances of i^6A_{37} $ACSL^{Phe}$ except that 2D NOESY spectra were also collected at 12, 18, and 32 °C. For the exchangeable resonances, 2D ^{15}N−^{1}H HSQC spectra were collected to identify ^{15}N−^{1}H chemical shift correlations. Two-dimen-

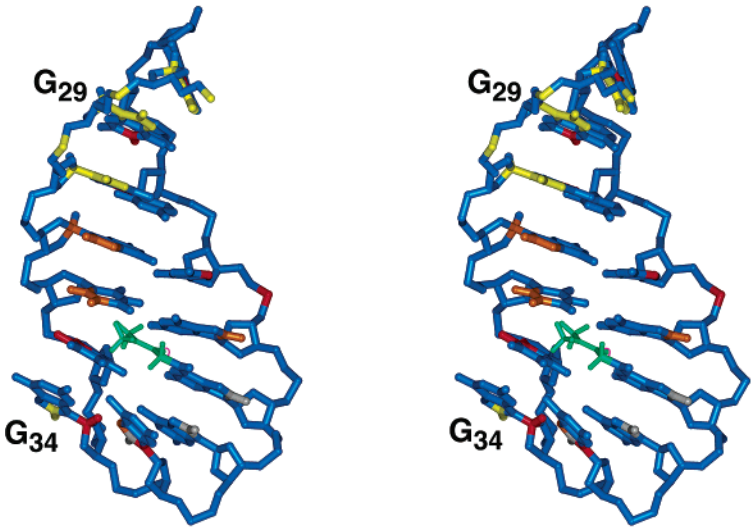

FIGURE 2: Stereoview of the ACSL^{Phe} highlighting sites of Mn^{2+} ion broadening. The strongest Mn^{2+} broadening effects (yellow) occur in the major groove of the stem. Medium to weak effects (orange to red) localize to nucleotides of the triloop and at the base of the stem. The dimethylallyl modification (green) and broadening effects unique to the modified anticodon stem−loop (gray) also are shown. The G34 C8 is very broadened in the modified RNA hairpin. The pattern of resonance broadening in the loop is accommodated by the solution structure of the unmodified ACSL^{Phe} and a delocalized Mn^{2+} ion.

sional ^{1}H−^{1}H NOESY experiments optimized separately for imino (NH) and amino (NH$_2$) proton resonances in ω_2 were acquired at 360 ms mixing time in 90% H$_2$O to obtain distance restraints involving the exchangeable protons.

^{13}C $T_{1\rho}$ relaxation times were measured using 2D ^{13}C−^{1}H ctHSQC-based experiments (*23*) separately optimized for C2, C6/8, and C1′ regions by centering the ^{13}C carrier at 152.6, 134.8, and 90.2 ppm, respectively. A 2.3 kHz ^{13}C spin lock field was used with delays of 4, 8, 12, 16, 24, 60, and 80 ms and 4, 8, 12, 16, 24, 44, 60, 80, and 120 ms for the C6/8 and C1′ measurements, respectively. The 12 and 24 ms experiments were collected twice to provide an estimate of the error of the measured intensities. The ^{13}C−^{1}H cross-peak volumes were fit to a single-exponential decay.

Modeling of Co(NH$_3$)$_6^{3+}$-Bound i^{6}A$_{37}$ ACSL^{Phe}. Semiquantitative distance constraints between nonexchangeable protons were estimated from cross-peak intensities in 2D NOESY and 3D ^{13}C-edited NOESY spectra. Using the covalently fixed pyrimidine H5−H6 distance (≈2.4 Å) as a reference, peak intensities were classified as strong, medium, weak, or very weak and their corresponding proton pairs given upper bound distance constraints of 3.0, 4.0, 5.0, or 6.0 Å, respectively. All distance constraints were given lower bounds of 0.0 Å. Distance constraints involving exchangeable protons were estimated from 180 ms mixing time NOESY spectra and were classified as either weak or very weak except for the intra-base-pair distances A·U H2−NH and G·C NH−NH$_2$, which were classified as strong constraints. The Watson−Crick base pairs G$_{27}$·C$_{43}$, G$_{28}$·C$_{42}$, G$_{29}$·C$_{41}$, G$_{30}$·C$_{40}$, and A$_{31}$·U$_{39}$ were constrained by 2.9 ± 0.3 Å between donor and acceptor heavy atoms and 2.0 ± 0.2 Å between acceptor and hydrogen atoms. Since the separation between the pairs U$_{33}$ 2′-OH, A$_{35}$ N7 and U$_{33}$ HN3, A$_{36}$ O1P could not be precisely determined from the NMR data, the hydrogen−heavy atom constraint distances were set to 2.2 ± 0.4 Å on the basis of crystallographically observed distances (*15*).

An initial set of structures was calculated for cobalt hexamine-bound i^{6}A$_{37}$ ACSL^{Phe} using X-PLOR 3.8.1 and a shortened version of the simulated annealing protocol previously described (*11*) in which the randomization step was omitted. The starting coordinates were derived from the solution structure of ACSL^{Phe} (*11*) and allowed to undergo 10 ps of constrained molecular dynamics followed by energy minimization. The dimethylallyl group was generated using Insight II (Accelerys) and parametrized as reported (*24*).

RESULTS

Localization of Metal Ion Binding Sites in the Anticodon Stem−Loop. Mg^{2+} produces chemical shift changes of stem and loop nucleotide resonances of both unmodified and A$_{37}$ N^6-prenylated ACSL^{Phe} molecules (Figure 1) (*11*). Mg^{2+} also broadens resonances in the loop of unmodified ACSL^{Phe} but sharpens some of the same resonances in the modified ACSL^{Phe}. These spectral changes point to the interaction of Mg^{2+} with the RNA molecules but do not allow precise localization of the metal ion binding site(s). Mn^{2+} and Co^{3+}-hexamine were used to better define the sites of metal ion association with the unmodified and modified ACSL^{Phe} molecules.

Mn^{2+} is a paramagnetic ion that causes a distance-dependent broadening of resonances for nuclei that are within a radius of ≈10 Å of the ion (*25*, *26*). MnCl$_2$ was titrated into Mg^{2+}-free solutions of 0.5 mM ACSL^{Phe} and i^{6}A$_{37}$ ACSL^{Phe}, and the resonance-specific broadening was monitored using 2D experiments. Figure 2 shows the distribution of Mn^{2+}-induced resonance broadening within the unmodified ACSL^{Phe}. In both molecules, the H8−C8 resonances of residues G$_{27}$−G$_{30}$ are extremely broad at 5 μM Mn^{2+}, and the NH resonances of G$_{28}$−G$_{30}$ are weakly broadened. In ACSL^{Phe}, the N7 and N9 resonances of G$_{28}$−G$_{30}$ are broadened beyond detection and the A$_{31}$ N7 is moderately broadened; the A$_{31}$ N9 is not affected. No other resonances of either molecule are affected at this concentration of Mn^{2+}. At 25 μM Mn^{2+}, the base resonances of G$_{27}$−G$_{30}$, including the NH resonances, are completely absent, and the base resonances of A$_{31}$−G$_{34}$ are broad in both molecules. The degree of broadening exhibited by residues A$_{31}$−G$_{34}$ of

Table 1: Mn^{2+}-Induced Resonance Broadening of $ACSL^{Phe}$ and i^6A_{37} $ACSL^{Phe}$ [a]

residue	H6−8/C6−8	H5/C5	H1′/C1′	H2/C2	H3′−P	P (1D)	H1/H3	N7	N9
G_{27}	++ (nd)		nd (nd)		+++	nd	+		
G_{28}	+++ (+++)		++ (+++)		+++	++	++	+++	+++
G_{29}	+++ (+++)		nd (+++)		+++	++	++	+++	+++
G_{30}	+++ (+++)		nd (+++)		+++	++	++	+++	+++
A_{31}	++ (+++)		− (++)	− (−)	++	nd		++	−
U_{32}	++ (+++)	++ (+++)	nd (−)		++	nd	−		
U_{33}	++ (+++)	++ (++)	nd (−)		++	nd	−		
G_{34}	++ (+++)		+ (nd)		−	nd	−		
A_{35}	− (+++)		− (−)	− (−)	−	−		++	+
A_{36}	− (+++)		− (nd)	− (−)	−	−		−	−
A_{37}	− (+++)		− (−)	− (nd)	−	−		−	−
A_{38}	++ (++)		nd (nd)	− (−)	−	−		−	−
U_{39}	− (−)	+ (−)	− (−)		−	−	−		
C_{40}	− (−)	− (+)	− (−)		−	−			
C_{41}	− (−)	− (−)	− (−)		−	nd			
C_{42}	− (−)	− (−)	− (−)		−	nd			
C_{43}	− (−)	− (−)	(−)			−			

[a] Mn^{2+} concentration of 25 μM. Key: (−) no broadening, (+) slight broadening, (++) intermediate broadening, (+++) peak broadened beyond detection, and (nd) not determined due to spectral overlap.

$ACSL^{Phe}$ is less than that observed for these residues in the i^6A_{37} $ACSL^{Phe}$ (Table 1). The H8−C8 resonances of A_{38} of both RNA molecules are moderately broadened. In i^6A_{37} $ACSL^{Phe}$, the C8−H8 resonances of A_{36}, A_{37}, and A_{38} are broad at 25 μM Mn^{2+}, and in $ACSL^{Phe}$, the H5−C5 resonances of U_{39} exhibit a small degree of broadening. None of the adenine H2 resonances of either molecule are affected at this concentration.

The sugar−phosphate backbone of the unmodified hairpin also was examined for possible interactions with Mn^{2+} ions using the $^{31}P-^{1}H$ HetCor experiment. The H3′ resonances of $G_{27}-G_{30}$ and the ^{31}P resonances of phosphates between residues G_{27} and A_{31} are extremely broadened. Mn^{2+} has a lesser effect on U_{32} and U_{33} H3′ resonances and caused no discernible broadening of either H3′ or ^{31}P resonances from G_{34} through C_{43}.

The resonance broadening from G_{27} to G_{30} is consistent with the known preference of Mn^{2+} for stretches of consecutive guanine nucleotides (*27*) (Figure 2). The N7 resonance is particularly sensitive to the interaction of the metal ion along the major groove. The effects on residues 38 and 39 suggest that there might also be a binding site in the loop region. It is unlikely that the effects on A_{38} and U_{39} are caused by the Mn^{2+} associated with $G_{27}-G_{30}$ since the resonances of atoms closer to these gaunine residues are not affected. For example, the A_{38} H2 of the unmodified hairpin is ≈2 Å closer to G_{30} N7 than A_{38} H8 and is not broadened. The cause of the differential broadening of A_{31} N7 and N9 is less certain but is presumably due to the relative proximity of the atoms to the paramagnetic center.

Localization of Metal Ion Binding Sites Using $Co(NH_3)_6^{3+}$. Cobalt hexamine has a size and coordination geometry that mimic those of hydrated Mg^{2+}, and thus the ion can be used to probe the interaction of RNA with Mg^{2+} through RNA−$Co(NH_3)_6^{3+}$ intermolecular NOEs (*26*, *28*). The base and 1′ chemical shifts of $ACSL^{Phe}$ and i^6A_{37} $ACSL^{Phe}$ were monitored during titration with $Co(NH_3)_6^{3+}$. Unlike the addition of Mn^{2+}, $Co(NH_3)_6^{3+}$ alters the chemical shifts of several resonances and necessitates reassignment of the $ACSL^{Phe}$ and i^6A_{37} $ACSL^{Phe}$ spectra. The resonances affected by Co-$(NH_3)_6^{3+}$ are largely the same for both molecules, although the magnitude of the chemical shift changes tends to be greater for i^6A_{37} $ACSL^{Phe}$.

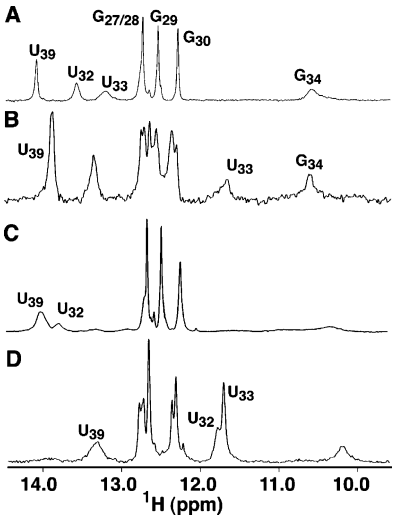

FIGURE 3: Imino ^1H spectra of $ACSL^{Phe}$ in (A) the absence and (B) the presence of 8 mM $Co(NH_3)_6^{3+}$ and i^6A_{37}-modified $ACSL^{Phe}$ in (C) the absence and (D) the presence of 8 mM $Co(NH_3)_6^{3+}$. Cobalt hexamine promotes a similar hydrogen-bonding pattern in the loop regions of both RNA molecules that differs from the triloop conformation. Although the prenyl group disrupts base pairing within the loop region, the modification stabilizes the cobalt hexamine-induced conformation.

Resonance assignments for the $Co(NH_3)_6^{3+}$-bound molecules were obtained using heteronuclear-based sequential assignment methods. The H3′, H4′, H5′, and H5″ were not assigned due to the broadness of many of the ribose resonances which led to very weak cross-peaks in 3D HCCH-TOCSY spectra. Cross-peak overlap in NOESY spectra permitted only partial assignment of these resonances. Several nonprotonated ^{15}N resonances were assigned through correlations to adenine H2, purine H8, and pyrimidine H6, and in the i^6A_{37} $ACSL^{Phe}$, 11 of the 16 interresidue ^{31}P resonances were assigned.

The NH proton resonances (Figure 3) were assigned using NOESY and $^{15}N-^{1}H$ HSQC spectra. All NH resonances except that of G_{34} are present in the HSQC spectrum. The N6 secondary amine of i^6A_{37} $ACSL^{Phe}$ also is present and was assigned from NOESY spectra through cross-peaks to the dimethylallyl resonances. The cytidine amino resonances were detected but could not be sequence specifically assigned

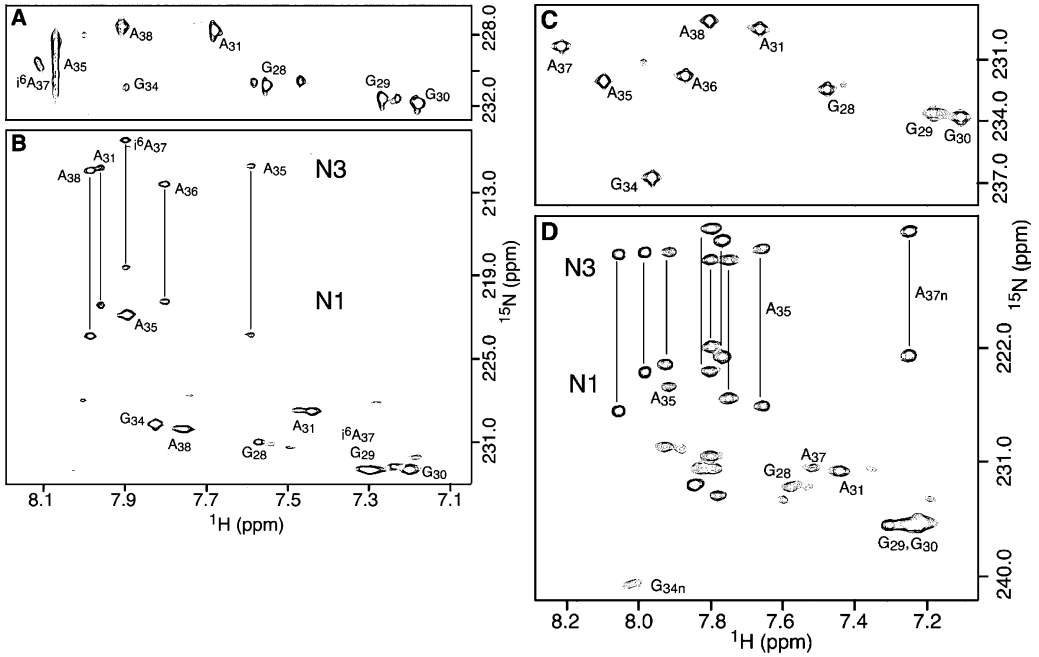

FIGURE 4: H8−N7 regions of the multiple-bond ^{1}H−^{15}N HSQC spectra of i^{6}A$_{37}$-modified ACSL^{Phe} in (A) the absence and (B) the presence of cobalt hexamine and unmodified ACSL^{Phe} in (C) the absence and (D) the presence of cobalt hexamine. The adenine H2−N1 cross-peaks also are present in (B) and (D). The A$_{35}$ N7 resonance of the modified hairpin is broadened by chemical exchange in the absence of cobalt hexamine but significantly sharpens and shifts ≈6 ppm upfield with the addition of the cation complex. Cobalt hexamine causes a similar change in the unmodified hairpin but also leads to additional conformation(s) of the loop nucleotides.

due to cross-peak overlap. The Co(NH$_3$)$_6^{3+}$ proton resonance is intense and has a chemical shift coincident with the literature value of 3.65 ppm (*28*).

Cobalt hexamine induces chemical shift changes for base and 1′ resonances of nucleotides G$_{28}$−U$_{39}$ of modified ACSL^{Phe}. The majority of H8, H6, and H1′ chemical shift perturbations are <0.3 ppm and frequently are in the downfield direction. The exceptions are the H8 resonances of A$_{36}$ and i^{6}A$_{37}$ and the H1′ resonances of A$_{36}$−U$_{39}$ which are shifted ≈0.8 ppm upfield and ≈0.4 ppm upfield, respectively. All of the adenine H2 and uridine H5 resonances shift downfield ≈0.2 ppm with the exception of A$_{36}$ and U$_{33}$ resonances, which do not change. The H2 resonance of i^{6}A$_{37}$ has a chemical shift of 7.90 ppm in the presence of cobalt hexamine but is broadened beyond detection in its absence. The A$_{35}$ N7 also is extremely broad in the absence of Co(NH$_3$)$_6^{3+}$, spanning 2.5 ppm, but resonates in the region characteristic of purine N7, between 226 and 232 ppm (Figure 4). In the presence of Co(NH$_3$)$_6^{3+}$, A$_{35}$ N7 resonates at 221.9 ppm and has a much narrower line width (Figure 4). All of the other purine N7 resonances cluster in the expected chemical shift region, downfield from 228 ppm. The G$_{28}$−G$_{30}$ NH resonance chemical shifts also are unaffected, but the U$_{32}$ NH resonance shifts upfield to 11.7 ppm and the U$_{33}$ NH resonance appears at 11.5 ppm (Figure 3). The majority of resonances of the ^{31}P spectrum remain clustered between −3.46 and −4.90 ppm in the presence of cobalt hexamine. However, the ^{31}P resonance corresponding to the G$_{34}$−A$_{35}$ phosphate linkage shifts downfield from −3.52 ppm to −2.76 ppm (Figure 5). A second downfield resonance (−0.45 ppm) is present and corresponds to a phosphate 5′ to G$_{28}$, G$_{29}$, U$_{33}$, G$_{34}$, i^{6}A$_{37}$, or A$_{38}$. These ^{31}P chemical shift changes could result from conformational changes of the phosphate backbone or from newly formed electrostatic or hydrogen bond interactions.

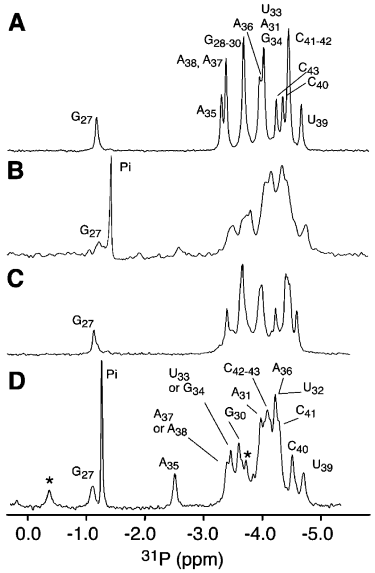

FIGURE 5: ^{31}P spectra of unmodified ACSL^{Phe} in (A) the absence and (B) the presence of 5 mM Co(NH$_3$)$_6^{3+}$ and i^{6}A$_{37}$-modified ACSL^{Phe} in (C) the absence and (D) the presence of 5 mM Co(NH$_3$)$_6^{3+}$. The phosphorus resonances are identified with the number of the residue immediately 3′ to the phosphate. Peaks marked with an asterisk are not sequence specifically assigned. The downfield-shifted resonances are consistent with *trans*-like α and ζ torsion angle changes. Mg^{2+} shifts some resonances also, but the displaced peaks are broad (*12*).

The Co(NH$_3$)$_6^{3+}$ protons have intense NOE cross-peaks with nucleotides on the 5′ strand of the stem and weak cross-peaks with those on the 3′ strand of the modified ACSL^{Phe}. Co(NH$_3$)$_6^{3+}$ has NOE cross-peaks of moderate intensity to the H8 and H6 of residues G$_{29}$−U$_{33}$ (mixing time of 360 ms) and the broadened NH$_2$ protons of residues C$_{40}$−C$_{43}$. The NH protons of G$_{28}$−G$_{30}$ and U$_{33}$ have intense cross-peaks with Co(NH$_3$)$_6^{3+}$. The G$_{34}$ H8, A$_{31}$ H2, A$_{35}$ H8, and

i^6A_{37} H2 resonances have weak cross-peaks to $Co(NH_3)_6^{3+}$. Together, these NOE interactions position a binding site for $Co(NH_3)_6^{3+}$ along the major groove of the stem distal to the loop. A second site of association exists on the major groove side of the loop but is less precisely defined by the pattern of NOEs. These binding sites are consistent with the locations identified using Mn^{2+}-induced broadening.

The chemical shift changes indicate multiple sites for interaction of cobalt hexamine along the RNA hairpin but also suggest that the ion may induce a conformational change in the loop region. Such a change is accompanied by increased stability of the RNA structure as resonances that are broadened by the dimethylallyl modification sharpen in the presence of $Co(NH_3)_6^{3+}$. Cobalt hexamine reduces the line widths of all of the uridine H5 and H6 and the dimethylallyl group proton resonances, but most notably the U_{33} H5 resonance decreases from 81 to 26 Hz. In contrast, the U_{39} NH resonance broadens, but its chemical shift does not change, and the G_{34} NH resonance broadens beyond detection. The resonances from nonexchangeable protons of these two nucleotides are not unusually broad, indicating that the G_{34} and U_{39} NH effects are probably due to accelerated solvent exchange of the NH protons rather than conformational exchange.

Cobalt Hexamine Alters the Structure of i^6A_{37} ACSL^{Phe}. The exchangeable proton NMR spectrum of i^6A_{37} ACSL^{Phe} points to cobalt hexamine-induced structural changes of the RNA. In the absence of $Co(NH_3)_6^{3+}$, the NH proton resonance of U_{33} is exchange broadened, and in unmodified ACSL^{Phe} its chemical shift is 13.2 ppm (Figure 3). With cobalt hexamine, the U_{33} NH resonance appears at 11.5 ppm and is intense (Figure 3). The U_{33} NH proton chemical shift and the protection of this proton from solvent exchange are consistent with participation of the proton in an intramolecular H−O hydrogen bond. The addition of cobalt hexamine also leads to appearance of a peak at 8.6 ppm. This ^{1}H resonance is not observed under sample conditions of 100% D_2O and does not exhibit one-bond ^{15}N or ^{13}C coupling (Figure 6). The only exchangeable resonance with such properties in RNA is the 2′-OH, but the 2′-OH protons often are in fast exchange with the solvent and generally are not observed. This 2′-OH resonance has weak NOE cross-peaks with U_{33} H6 and A_{35} H8 and strong NOEs with U_{33} H1′ and U_{33} H2′ and was identified as the U_{33} 2′-OH (Figure 6). Notably, U_{33} NH and 2′-OH protons form the hydrogen bonds that stabilize the U-turn of fully modified yeast tRNA^{Phe} (Figure 7).

The chemical shifts of the A_{35} N7 and 5′-pA_{35} ^{31}P resonances also suggest a structural change. In the absence of cobalt hexamine, the A_{35} base is stacked beneath A_{36} and i^6A_{37}, and the N7 is solvent exposed (Figure 2). The >6 ppm upfield shift of the A_{35} N7 resonance upon $Co(NH_3)_6^{3+}$ binding indicates creation of a stable hydrogen bond involving the N7 (*29*). In yeast tRNA^{Phe}, this atom serves as the hydrogen bond acceptor of the U_{33} 2′-OH (Figure 7). The ^{31}P resonance corresponding to the phosphate between G_{34} and A_{35} resides in the main cluster of resonances but shifts downfield with addition of $Co(NH_3)_6^{3+}$ (Figure 5). Another peak also shifts downfield but could not be assigned. One possibility for these shifts is a conformational change about the phosphate backbone, but the formation of ionic or hydrogen bond interactions cannot be excluded.

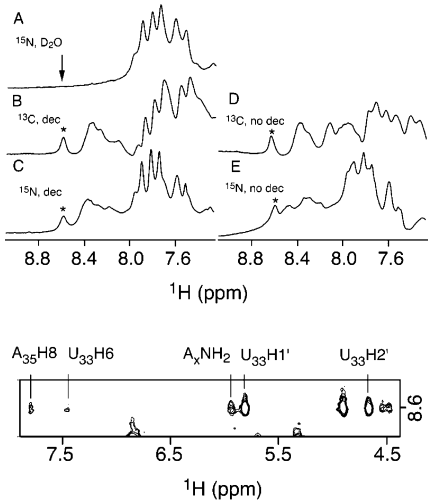

FIGURE 6: Spectra of i^6A_{37} ACSL^{Phe} in the presence of 8 mM $Co(NH_3)_6^{3+}$. Spectra were collected at 5 °C in 99.9% D_2O (A) or 90% H_2O (B−E). The isotope enrichment (^{13}C and ^{15}N) of the samples and whether decoupling was applied are indicated (B−E). The proton resonating at 8.6 ppm was determined to be a 2′-OH since it is exchangeable and exhibits no one-bond ^{13}C or ^{15}N coupling. The sequence-specific assignment of this resonance to U_{33} was determined from cross-peaks to the resonance in the NOESY spectrum (bottom). The identity of the A−NH_2 cross-peak could not be determined. The slow-exchange properties of this 2′-OH proton and its chemical shift are consistent with the U_{33} 2′-OH−A_{35} N7 hydrogen bond characteristic of the U-turn.

These spectral features demonstrate that the modified RNA hairpin does not maintain the triloop conformation in the presence of $Co(NH_3)_6^{3+}$. However, the small number of experimental constraints that can be reliably extracted do not support the calculation of a high-resolution structure. Thus, the conformation of the loop was modeled beginning with the coordinates of the structure of unmodified ACSL^{Phe} using a limited simulated annealing protocol and semi quantitative distance constraints. Residues 32−38 of i^6A_{37} ACSL^{Phe} were constrained using 50 NOE-derived distances. No ribose puckers or torsional angles were constrained for these residues due to the mixed C2′/C3′-endo character of the ribose moieties. The model generated using these constraints has the 3′ base-stacked pattern of nucleotides A_{35} through i^6A_{37}, and the phosphate backbone turns sharply between U_{33} and G_{34} (Figure 8).

Base−base and interresidue base−ribose NOEs are contiguous from G_{27} to U_{32}, and the intensities of the base−ribose NOEs are consistent with C3′-endo ribose puckers. The continuity of the sequential NOEs is broken between U_{33} and G_{34}, unlike the unmodified metal-free molecule, indicating that these bases do not stack. On the 3′ half of the stem−loop and beginning with G_{34}, the sequential H6/8 NOE connectivities are contiguous. The H2 of each adenine residue has a moderately intense NOE with the H1′ of the 5′-flanking nucleotide at a NOESY mixing time of 180 ms. Only the A_{31} H2 resonance has a cross-strand NOE involving an H1′ resonance (C_{40} H1′); there are no cross-strand H2 to H1′ NOEs for residues A_{35}−A_{38}. This is in contrast to spectra of the cobalt-free molecule which exhibit cross-strand NOEs U_{33} H1′−A_{38} H2 and A_{31}H2−C_{40}H1′ and suggests that the regular A-form helix terminates at the A_{31}·U_{39} base pair in the cobalt-bound molecule. In addition, the nonsequential NOE cross-peaks U_{33} H1′−A_{35} H8 and U_{33} H1′−A_{36} H8 are

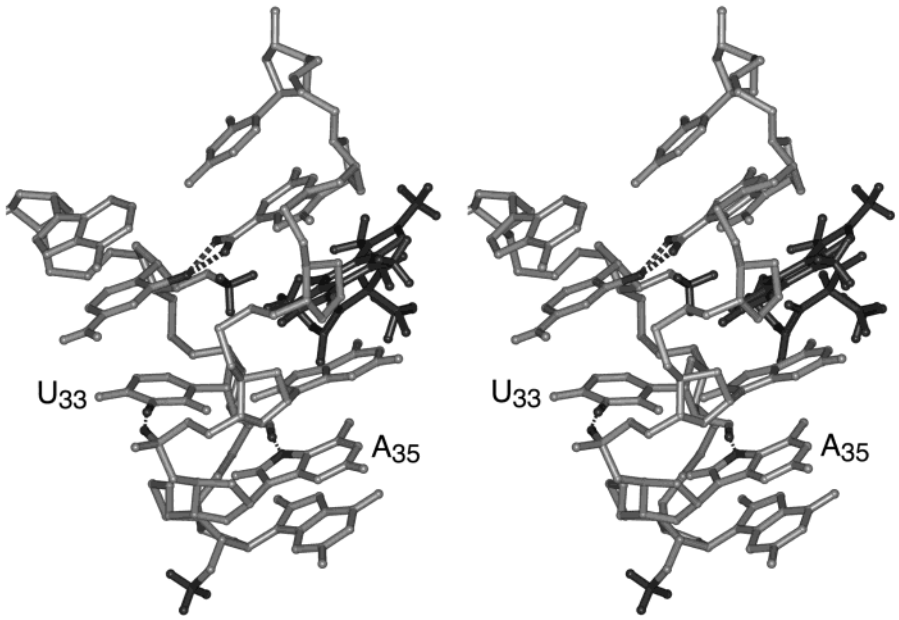

FIGURE 7: Crystal structure of residues 31−39 of yeast $tRNA^{Phe}$. Modifications within the anti-codon stem−loop are highlighted in dark. The 3′-stack of the anticodon bases and the U_{33} 2′-OH−A_{35} N7 and U_{33} HN3−A_{36} O1P hydrogen bonds characterize the U-turn motif.

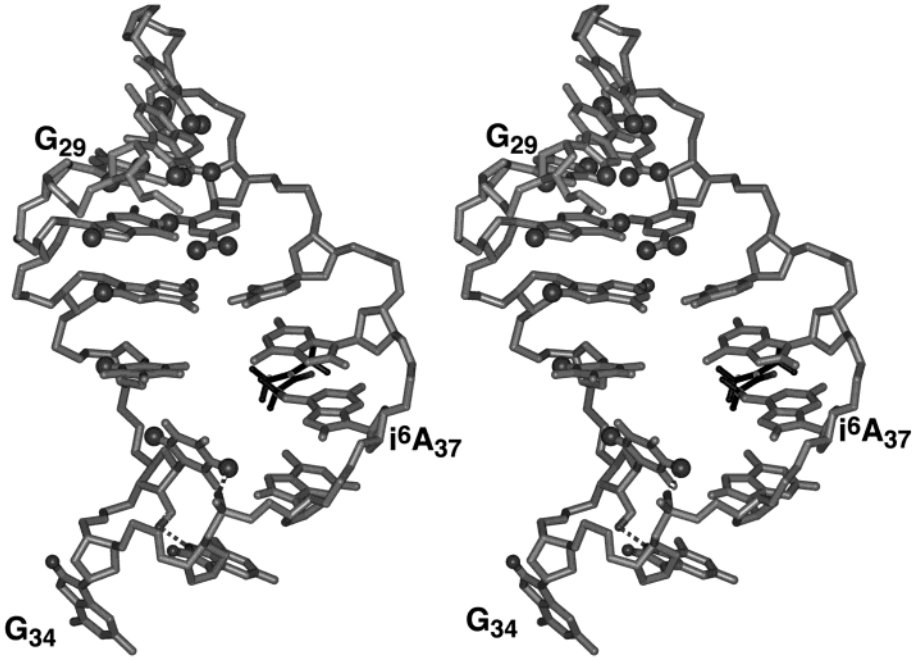

FIGURE 8: Stereoview of residues 28−42 of the i^6A_{37} $ACSL^{Phe}$ in the presence of $Co(NH_3)_6^{3+}$. Spheres indicate protons that give rise to NOEs with $Co(NH_3)_6^{3+}$, and the dimethylallyl modification of A_{37} is shown in dark. The U_{33} 2′-OH−A_{35} N7 and U_{33} HN3−A_{36} O1P hydrogen bonds deduced from chemical shift and exchange data are shown as dashed lines. The diffusion of intermolecular NOEs within the loop region does not allow precise localization of the $Co(NH_3)_6^{3+}$.

very weak in the metal-free spectrum but have moderate intensity when $Co(NH_3)_6^{3+}$ is present, reflecting the proximity of these bases. Finally, a parallel stacked arrangement of the A_{35} and A_{36} bases is supported by a moderately intense H2−H2 NOE.

The sugar−phosphate backbone of the loop also undergoes conformational rearrangement with $Co(NH_3)_6^{3+}$. The intraresidue G_{34}, A_{36}, and i^6A_{37} H8 to H2′ NOE cross-peaks are very weak, and the intraresidue A_{35} H8−H2′ NOE cross-peak has medium intensity but is clearly weakened in the presence of $Co(NH_3)_6^{3+}$. The intensities of the sequential H2′−H8 connectivities for residues 34−39 increase with $Co(NH_3)_6^{3+}$. The C1′ resonances of loop residues 34−37 sharpen and shift downfield into the main cluster of 1′ resonances. These relative NOE intensities and the downfield shifts of the C1′ resonances are consistent with a shift of the ribose puckers from the C2′-endo conformation to the C3′-endo conformation. This conformational change is further supported by the loss of H1′−H2′ cross-peaks from the DQF-COSY spectrum, although the increased line width could also contribute to their absence.

The binding of $Co(NH_3)_6^{3+}$ to i^6A_{37} $ACSL^{Phe}$ does not significantly alter the NOE cross-peak pattern of the dimethylallyl protons. There are cross-strand NOEs from the methyl protons to U_{32} H2′, U_{33} H1′, U_{33} H6, and U_{33} H5′. The CH_3−H5′ interaction is particularly intense, and the A_{38}

Table 2: C2, C6, C8, and C1′ $T_{1\rho}$ Relaxation Times for the i^6A_{37} $ACSL^{Phe}$ RNA Molecule in the Presence of $Co(NH_3)_6^{3+}$

	$Co(NH_3)_6^{3+}$ $T_{1\rho}$ (ms)[b]		
residue[a]	C6/C8	C1′	C2
G_{27}			
G_{28}	38.9	46.4	
G_{29}	39.6	45.7	
G_{30}	38.2	46.2	
A_{31}	38.2	50.0	40.2
U_{32}	33.5	46.1	
U_{33}	34.0	46.6	
G_{34}	42.4	49.8	
A_{35}	42.1	51.1	35.9
A_{36}	37.2	47.5	36.1
A_{37}	36.3	49.9	39.3
A_{38}	32.3	42.8	38.3
U_{39}	32.2	48.5	
C_{40}	35.8	47.3	
C_{41}	35.4	49.9	
C_{42}	33.2	46.6	
C_{43}	32.6	45.6	

[a] The transcription reactions were primed with 5′-GMP, resulting in incomplete labeling of the 5′-terminal nucleotide and preventing the G_{27} C8 and C1′ relaxation rates from being measured. [b] The uncertainty in the measured relaxation times is ±5%.

H2 has intense NOEs to both of the methylene protons. These NOEs limit the conformational freedom of the prenyl group within the loop region. It should be noted that Mg^{2+} also does not lead to significant changes of the pattern of cross-peaks involving the prenyl group.

Dynamics of the Modified Hairpin Molecule with Co-$(NH_3)_6^{3+}$. The reorientation of a $^{13}C-^1H$ bond vector on the picosecond time scale is reflected by its carbon $T_{1\rho}$ relaxation: the longer the relaxation time, the more mobile the $^{13}C-^1H$ pair. The $T_{1\rho}$ relaxation times for the adenine C2, base C6/8, and ribose C1′ positions of i^6A_{37} $ACSL^{Phe}$ were measured to determine the effects of $Co(NH_3)_6^{3+}$ on the fast time scale dynamics of the RNA molecule (Table 2). In the presence of $Co(NH_3)_6^{3+}$, the C8 nuclei of G_{34} and A_{35} have relaxation times 15−20% longer than all other purines in the molecule. The relaxation times of the pyrimidine C6 nuclei are largely uniform throughout the RNA molecule. The majority of the C1′ nuclei in the loop region relax at rates comparable to those in the stem region. This is in contrast to the C1′ relaxation rates of the metal-free unmodified molecule in which the G_{34} and A_{37} relax significantly faster (*11*). The most notable exception is the A_{35} C1′, but its relaxation time is only slightly extended compared to the other C1′ atoms in the molecule. The relative uniformity of the relaxation times throughout the molecule suggests that the motional properties of all residues are similar. This is consistent with a well-ordered and stable loop structure since the stem nucleotides of the i^6A_{37} $ACSL^{Phe}$ are unlikely to exhibit a high degree of flexibility. Resonance broadening and contributions from chemical exchange prevented an accurate measurement of the $T_{1\rho}$ relaxation times in the presence of Mg^{2+}.

Spectral and Structural Effects of Co$(NH_3)_6^{3+}$ on Unmodified $ACSL^{Phe}$. The unmodified $ACSL^{Phe}$ has a reduced affinity for cobalt hexamine so that chemical shift changes and NOE patterns similar to those induced in i^6A_{37} $ACSL^{Phe}$ require higher concentrations of the metal ion. For example, the A_{36} and A_{37} H8 resonances achieve their maximum chemical shift change at a $Co(NH_3)_6^{3+}$ concentration 5-fold higher than that

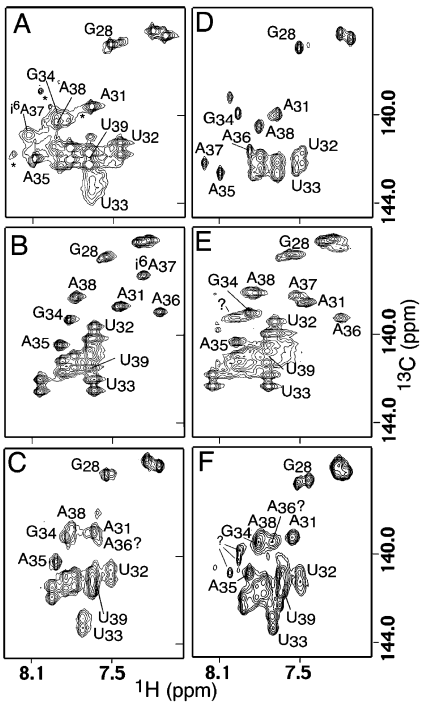

FIGURE 9: Base 6/8 regions of 2D $^{13}C-^1H$ HMQC spectra of (A−C) i^6A_{37}-modified $ACSL^{Phe}$ and (D−F) unmodified $ACSL^{Phe}$: (A, D) without $Co(NH_3)_6^{3+}$ or Mg^{2+}, (B, E) with 8 mM $Co(NH_3)_6^{3+}$, and (C, F) with 8 mM Mg^{2+}. The broadened resonances indicate that modification of A_{37} and addition of Mg^{2+} or $Co(NH_3)_6^{3+}$ destabilize the loop region of the $ACSL^{Phe}$. However, Mg^{2+} and cobalt hexamine act in synergy with the prenyl modification and stabilize the structure of the $ACSL^{Phe}$ loop. The redistribution of chemical shifts caused by cobalt hexamine points to a loop conformation that is different from the metal-free $ACSL^{Phe}$.

used for i^6A_{37} $ACSL^{Phe}$. Also, there are $ACSL^{Phe}$ resonances that have broad line widths in the presence of $Co(NH_3)_6^{3+}$ that are indicative of intermediate exchange.

The spectra of the unmodified $ACSL^{Phe}$ exhibit many of the $Co(NH_3)_6^{3+}$-induced features observed for i^6A_{37} $ACSL^{Phe}$, but the spectra also indicate that cobalt hexamine causes multiple conformations of the RNA molecule. Whereas a single set of resonances is observed in spectra of the modified $ACSL^{Phe}$, several loop nucleotide resonances of the unmodified $ACSL^{Phe}$ exhibit broadening or are split into major and minor resonance pairs in the presence of cobalt hexamine (Figures 4 and 9). The chemical shift differences between the major set of resonances and the corresponding resonances of the metal-free RNA molecule parallel the differences between resonances of i^6A_{37} $ACSL^{Phe}$ and $Co(NH_3)_6^{3+}$-bound i^6A_{37} $ACSL^{Phe}$. However, the magnitudes of the chemical shift changes tend to be greater for nucleotides proximal to the modification site in i^6A_{37} $ACSL^{Phe}$, particularly the H8 resonances of A_{36}, A_{37}, and A_{38} and the H2 of i^6A_{37}.

The NOE patterns for the modified and unmodified $ACSL^{Phe}$ molecules also are similar in the presence of cobalt hexamine. The sequential base−1′ NOE connectivity is broken between G_{34} and A_{35}, and there is a nonsequential U_{33} H1′−A_{35} H8 NOE. Further, the A_{31} H2−C_{40} H1′ NOE is the only cross-strand NOE involving an H2 resonance; the H2 resonances of A_{35} through A_{38} exhibit NOE cross-peaks only to H1′ resonances of sequential nucleotides. The C1′ resonances of residues $G_{34}-A_{37}$ are shifted downfield and point to a loss of C2′-endo character. The A_{35} N7

resonance is shifted upfield to 220.3 ppm but is weak relative to the N7 resonance of the modified molecule (Figure 4). The U_{33} 2′-OH resonance is not observed in spectra of the $Co(NH_3)_6^{3+}$-bound $ACSL^{Phe}$. The NH resonances of U_{32} and U_{33} also shift upfield as they do in the modified molecule but are broad (Figure 3).

The spectra also demonstrate that cobalt hexamine affects the modified and unmodified RNA hairpins differently. For the unmodified hairpin in the presence of cobalt hexamine, the bases of nucleotides U_{32}, U_{33}, and U_{39} have two sets of resonances (Figure 9). The adenine H2 and purine H8 resonances of loop nucleotides also exhibit doubling (Figure 4), indicating that the loop region exists in two or more conformations that are in slow exchange. This resonance doubling is not present in spectra of the i^6A_{37} $ACSL^{Phe}$ molecule. Thus $Co(NH_3)_6^{3+}$ by itself is not sufficient to organize the loop region of unmodified $ACSL^{Phe}$ into one stable conformation.

DISCUSSION

Divalent metal ions and modified nucleoside bases extend the structural and functional diversity of RNA molecules. Metal ions participate in RNA folding, structure stabilization, and RNA-mediated catalysis. Base modifications can alter the chemical and electrostatic properties of RNA molecules and create unique opportunities for nonstandard interactions. We have chosen the $ACSL^{Phe}$ from *E. coli* as a system to examine in detail the interactions between ions and base modifications and their individual and combined effects on RNA structure. This study demonstrates that these interactions are important to form the U-turn motif within the sequence context of the *E. coli* $ACSL^{Phe}$.

The Hydrogen Bond Pattern of the U-Turn Is Reflected in the Chemical Shifts of the Paired Atoms. The U-turn motif was first revealed by the crystal structure of fully modified yeast $tRNA^{Phe}$ (*13*) and is characterized by an abrupt change in the direction of the phosphate backbone. The motif is stabilized by cross-strand hydrogen bonds, but stacking of bases that follow the turning phosphate may also contribute stability. In the anticodon stem−loop, the first nucleotide of the turn, U_{33}, forms hydrogen bonds between the U_{33} NH and the *pro-R*(p) phosphoryl oxygen (O1P) of the phosphate preceding A_{36} and between the U_{33} 2′-OH and the N7 of A_{35} (*13*). This cross-strand hydrogen bond pattern is a hallmark of the UNR class of U-turns. Only in the presence of $Co(NH_3)_6^{3+}$ does the dimethylallyl-modified molecule show spectral evidence supporting all of the above structural characteristics. The spectra of the unmodified molecule in the presence of $Co(NH_3)_6^{3+}$ also show effects of a tight turn, base stacking and hydrogen bonding, but as one of at least two conformations.

In solution studies of RNA molecules, non-Watson−Crick hydrogen bond interactions often have been inferred on the basis of the proximity of donor−acceptor pairs in calculated structures. Although scalar correlation of the participating heavy atoms may not be possible, these hydrogen bonds can produce characteristic spectral signatures. In the $Co(NH_3)_6^{3+}$-bound i^6A_{37} $ACSL^{Phe}$, the 2′-OH of U_{33} is protected from rapid exchange with solvent and has a chemical shift of 8.60 ppm. The putative acceptor atom, A_{35} N7, has a chemical shift that is >6 ppm upfield from the main cluster of purine N7 resonances. Base pairing of adenine was shown to cause a large upfield shift of the N1 resonance in duplex DNA (*29*), and an ≈6 ppm upfield shift has been observed for adenine N1 resonances hydrogen bonded to 2′-OH protons (*30*). The relative shift of the N7 resonance appears to be dependent upon the identity of the H-bond donor, though. The sheared G·A base pair produces a *downfield* shift of the N7 resonance, but the adenine N7 of a sheared G·A pair participates in a hydrogen bond with the exocyclic NH_2 of the partner guanine base (*31*). The Hoogsteen A·U base pair, which involves a U N3H−A N7 hydrogen bond, also leads to a downfield shift of the N7 resonance (*30*). Observation of 2′-OH resonances in RNA is atypical and usually occurs when the 2′-OH forms a hydrogen bond that is sequestered from the solvent. Interestingly, the majority of 2′-OH protons identified in RNA and simple carbohydrates resonate around 6.1−6.9 ppm, upfield of the U_{33} 2′-OH (*27*, *32*−*35*). However, the chemical shift of the U_{33} 2′-OH is similar to those observed for 2′-OH protons in the luteoviral P1−P2 frame-shifting pseudoknot (*30*).

The U_{33} NH position also has unusual spectral properties. The NH proton is protected from rapid solvent exchange, and its chemical shift of 11.5 ppm is consistent with an oxygen−NH hydrogen bond. The U_{33} NH resonance is intense and has NOEs with A_{36} H8, A_{35} H1′, and A_{37} H2 or A_{35} H8. Our efforts to obtain through-bond NH−P correlations and 2′-OH−N7 correlations were not successful, possibly due to the line widths of the NH and 2′-OH peaks (20 and 30 Hz, respectively) and presumably small scalar coupling constants. Nonetheless, the exchange properties of these protons and the chemical shifts of these resonances appear to be diagnostic of the crystallographically defined hydrogen bond network (*1*, *2*).

The U-turn motif has been reported for several RNA stem−loop sequences other than the yeast $tRNA^{Phe}$ anticodon, and some of these employ alternative hydrogen bond pairs to stabilize the turn (*3*, *8*, *18*, *36*). In GNRA tetraloops, their is a sharp turn of the phosphate backbone immediately following the G nucleotide. The hydrogen bond network within the GNRA loop is more extensive, but the geometry of the U_{33} interactions is conserved. The G NH_2 and 2′-OH groups functionally substitute for the U_{33} NH and 2′-OH groups, donating protons to the R N7 and RpA phosphate acceptor atoms (*3*). In *E. coli* $tRNA^{Cys}$ (anticodon GCA), U_{33} and C_{35} form a turn-stabilizing hydrogen bond that is functionally equivalent to the U_{33}−A_{35} interaction of $tRNA^{Phe}$, but the donor−acceptor roles are reversed. The exocyclic NH_2 group of C_{35} donates the proton to the U_{33} O2′ and preserves the ability of C_{35} to form Watson−Crick base pair interactions (*36*). In the modified ACSL of *E. coli* $tRNA^{Lys}$ (anticodon mnm^5s^2-UUU), only the U_{33} NH−O1P hydrogen bond interaction is maintained (*18*). The 2′-OH of U_{33} does not form an intramolecular hydrogen bond, but the absence of this bond may be compensated by interactions of modifications on U_{34} and A_{37}. Thus, the hydrogen bond pairs that help to stabilize the U-turn can provide direct support for the motif in solution through a characteristic set of spectal signatures involving exchangeable protons and ^{15}N or ^{31}P chemical shifts.

The ACSL Associates Weakly with the Metal Ions. The hydrated Mg^{2+} binding properties of unmodified and i^6A_{37}-modified $ACSL^{Phe}$ hairpins were examined using the divalent

Mn^{2+} and the trivalent $Co(NH_3)_6^{3+}$. Mn^{2+} broadens resonances between G_{27} and G_{34} of the unmodified hairpin in addition to A_{38} on the 3′ strand of the stem, but the strongest effect is localized to $G_{28}-G_{30}$. In addition to the resonances corresponding to the same stem nucleotides, the prenylated molecule exhibits resonance broadening from U_{32} to A_{38} with A_{35}, A_{36}, and i^6A_{37} being most affected. The amine protons of $Co(NH_3)_6^{3+}$ have NOE cross-peaks to residues in the stem and along the 5′ half of the loop region (H6/8 of $G_{29}-U_{33}$) of the modified hairpin. $Co(NH_3)_6^{3+}$ also has an NOE to the A_{35} H8. The Mn^{2+} broadening patterns and the distribution of the cobalt hexamine NOE cross-peaks indicate that these ions localize to the major grooves of both RNA hairpins and to the loop region of the modified $ACSL^{Phe}$ but are not sufficiently restrictive to permit identification of unique coordination sites.

The $ACSL^{Phe}$ contains features that accommodate the binding modes of Mg^{2+}, Mn^{2+}, and $Co(NH_3)_6^{3+}$ ions. The interactions of these ions with RNA often involve the O6 and N7 atoms of guanine nucleotides and can include the phosphoryl oxygens of the backbone (*25*, *37*−*39*). The sequential guanine residues of the stem create an electronegative surface along one side of the major groove and provide a scaffold of hydrogen bond acceptors. The binding of Mn^{2+} and $Co(NH_3)_6^{3+}$ ions at three or more sequential G·C base pairs has been observed for other RNAs (*25*, *28*, *39*), but the affinity of these sites is low compared to helices containing tandem G·U base pairs (*28*). Although the U-turn motif is stabilized by less than a 3:1 ratio of $Co(NH_3)_6^{3+}$:RNA in the modified hairpin, the cobalt hexamine complex could not be uniquely positioned in the loop region. The RNA−$Co(NH_3)_6^{3+}$ NOEs are distributed over several residues and suggest that localization of the ion within the loop region does not involve site-specific coordination to the RNA. The orthorhombic crystal form of yeast $tRNA^{Phe}$ contains a Mg^{2+} in the anticodon loop that is situated between A_{38} N7 and the Y_{37} O1P (*14*). However, the octahedral coordination of this Mg^{2+} is not resolved and suggests that the ion is not rigidly fixed. No $Co(NH_3)_6^{3+}$ ions have been identified in the anticodon loop region of yeast crystalline $tRNA^{Phe}$ (*39*), but G_{34} N7 and the phosphoryl oxygen of the 5′ flanking phosphate coordinate a Co^{2+} in the monoclinic form of the crystal (*14*). However, the Co^{2+} interaction involves inner-sphere coordination and thus is unlikely to serve a significant role in the cobalt hexamine-stabilized conformation.

The chemical shift and line width changes and the NOE patterns generated by $Co(NH_3)_6^{3+}$ are similar to those observed for Mg^{2+} and indicate that cobalt hexamine can effectively substitute for Mg^{2+}. Although the magnitudes of the Mg^{2+}-induced chemical shift changes are predictably smaller than those produced by $Co(NH_3)_6^{3+}$, the $U_{33}-A_{35}$ NOE cross-peaks, which are expected to result from a U-turn fold, are of comparable intensity with Mg^{2+} and $Co(NH_3)_6^{3+}$. Also, like cobalt hexamine, Mg^{2+} leads to multiple conformations among loop nucleotides of the unmodified $ACSL^{Phe}$ while both ions lead to a single set of resonances for the modified $ACSL^{Phe}$. This effect is consistent with fluorescence studies using fully modified yeast $tRNA^{Phe}$ showing that Mg^{2+} stabilizes one of three conformations of the anticodon stem−loop (*40*). However, Mg^{2+} does not produce the hydrogen bond spectral signatures for a U-turn that are observed with $Co(NH_3)_6^{3+}$. The inability of Mg^{2+} to fully mirror the RNA organizational effect of $Co(NH_3)_6^{3+}$ could be attributed to its reduced charge density relative to cobalt hexamine.

Although $Co(NH_3)_6^{3+}$ and hydrated Mg^{2+} ions share coordination geometry and are of similar size, only $Co(NH_3)_6^{3+}$ appears to stabilize the U-turn motif. These results are consistent with the nonlinear Poisson−Boltzmann model used to describe Mg^{2+} binding to tRNA (*41*). The di- and trivalent ions cluster in a region of high negative electrostatic potential, such as that created by the turn of the phosphate backbone (*42*). The higher positive charge of $Co(NH_3)_6^{3+}$ leads to a stronger electrostatic effect when interacting with the RNA. This is consistent with the ≈10-fold higher affinity of $Co(NH_3)_6^{3+}$ for nucleic acids (*26*, *43*). The increased charge may better neutralize repulsion of the phosphate backbone and permit collapse of the loop into the U-turn. Analogously, $Co(NH_3)_6^{3+}$ has been shown to stabilize the A-form geometry in DNA helices whereas Mg^{2+} does not (*44*, *45*). The phosphate−phosphate distance is shorter for A-form geometry than for B-form geometry, and charge neutralization by $Co(NH_3)_6^{3+}$ is capable of inducing the B-to-A helix transition (*45*).

Synergy between Metal Ion Binding and Base Modification. The binding of cobalt hexamine to i^6A_{37} $ACSL^{Phe}$ substantially alters the structure and stability of loop region nucleotides, converting the dynamic loop into a stable U-turn. The well-organized triloop of $ACSL^{Phe}$ also changes in the presence of $Co(NH_3)_6^{3+}$, but the U-turn is only one of several dynamic folds that the nucleotides sample in the loop region. The inability of $Co(NH_3)_6^{3+}$ to induce formation of a single nonexchanging conformation in the unmodified hairpin indicates that the dimethylallyl group of i^6A_{37} either enhances the binding of cobalt hexamine by organizing a favorable environment for coordination of the metal ion complex or destabilizes alternate conformations of the unmodified loop that thermodynamically compete with the U-turn. $Co(NH_3)_6^{3+}$, Mg^{2+}, and i^6A_{37} cause similar spectral effects for $ACSL^{Phe}$ that indicate disruption of the U_{33}·A_{37} and U_{32}·A_{38} base pairs and creation of structural heterogeneity (*11*). These effectors clearly destabilize the triloop and establish a conformational landscape with shallow energy wells. However, the $ACSL^{Phe}$ requires more than 15 equiv of $Co(NH_3)_6^{3+}$ to produce maximum change and stability of the loop conformation whereas the i^6A_{37} $ACSL^{Phe}$ requires only 3 equiv of $Co(NH_3)_6^{3+}$. These results suggest that the dimethylallyl modification promotes the U-turn conformation by destabilizing the triloop, presumably through disruption of intraloop hydrogen bonds.

Folding of RNA and maintenance of tertiary structure have been linked to the aggregate effects of base modification and Mg^{2+} binding at other positions in tRNA (*19*, *46*, *47*). At position 40 of yeast $tRNA^{Phe}$, 5-methylcytidine enables the cooperative binding of Mg^{2+} to the anticodon stem−loop. At a concentration of 0.1 mM, Mg^{2+} induces a conformational change in the loop region that is not observed in the absence of the modification (*46*). Mg^{2+} has also been implicated in altering the conformation of the modified residue Y_{37} of yeast $tRNA^{Phe}$ by promoting its stacking (*40*). The unmodified yeast $tRNA^{Phe}$ adopts a nativelike tertiary fold, but requires >10 times more Mg^{2+} to maintain its global structure than the fully modified form (*48*). The structural

integrity of the D-stem and of D-loop:T-loop tertiary interactions of unmodified $tRNA^{Val}$ requires a >20-fold molar excess of Mg^{2+} (*19*), but these structure elements are stabilized without added Mg^{2+} in the fully modified molecule (*19*).

The U-turn motif is important for ribosome binding of tRNA. Although the closed form of the anticodon loop from *E. coli* $tRNA^{Phe}$ is relaxed by Mg^{2+} and dimethylallyl modification of A_{37} (*11*), intermolecular interactions in the context of the translational machinery can stabilize an open loop conformation of the *E. coli* $ACSL^{Phe}$ in the absence of modifications. Crystallographic data show that the unmodified $ACSL^{Phe}$ maintains a U-turn motif when bound to a complex of the 30S subunit and mRNA (*49*). This conformation appears to be stabilized by a network of hydrogen bonds that includes codon−anticodon base pairing. U_{33} does not appear to form direct intermolecular contacts (*49*), but modification or substitution of U_{33} can reduce the affinity of the anticodon stem−loop for the ribosome (*50*, *51*). U_{33} base or ribose substitutions that prevent the N3H−O1P or 2′-OH−N7 hydrogen bonds or fix the ribose pucker or the conformation of the glycosidic bond lower the affinity between yeast $tRNA^{Phe}$ and the ribosome. However, the severity of the inhibitory effects can be partially mitigated by natural modifications within the ACSL (*51*). Thus, although the translational effect of forming a stable U-turn motif prior to ribosome binding has not been quantified, the importance of this conformation on the ribosome is established.

For the *E. coli* $ACSL^{Phe}$, we have shown here that the combined effects of base modification and charge neutralization by multivalent cations are synergistic and promote U-turn formation within the loop. Mg^{2+} does not stabilize the U-turn as effectively as cobalt hexamine in i^6A-modified and unmodified $ACSL^{Phe}$ molecules, but the fully modified stem−loop contains three other modifications: ψ_{32}, ψ_{39}, and ms^2A_{37}. The substitution of ψ_{39} with U_{39} within the context of fully modified $tRNA^{Phe}$ disrupts the secondary structure of the anticodon stem proximal to the loop (*52*), and the methylthio modification of C2 can improve stacking of the anticodon bases within the mRNA−tRNA minihelix (*53*). Mutagenesis experiments demonstrate that these modifications are important for normal cell growth (*54*−*56*). However, these mutations affect modification of multiple tRNA species. Of these base modifications, pseudouridine is the most abundant and most studied. A conserved pseudouridine within the branch-point helix of the 5′ splice site of pre-mRNA causes an unpaired adenine on the opposite strand to loop out of the helix rather than stack (*57*). Thus, additional modifications of i^6A_{37} $ACSL^{Phe}$ may contribute properties that allow Mg^{2+} to stabilize the overall architecture of the loop or may in themselves lead to a stable U-turn.

ACKNOWLEDGMENT

We thank M. Michnicka for preparation of the T7 RNA polymerase and isotopically labeled 5′-NTPs.

SUPPORTING INFORMATION AVAILABLE

Two tables listing chemical shifts of the cobalt hexamine-bound i^6A_{37} $ACSL^{Phe}$ RNA molecule. This material is available free of charge via the Internet at http://pubs.acs.org.

REFERENCES

1. Kim, S. H., Suddath, F. L., Quigley, G. J., McPherson, A., Sussman, J. L., Wang, A. H., Seeman, N. C., and Rich, A. (1974) Three-dimensional tertiary structure of yeast phenylalanine tranfer RNA, *Science 185*, 435−440.
2. Robertus, J. D., Ladner, J. E., Finch, J. T., Rhodes, D., Brown, R. S., Clark, B. F. C., and Klug, A. (1974) Structure of yeast phenylalanine tRNA at 3 Å resolution, *Nature 250*, 546−551.
3. Jucker, F. M., Heus, H. A., Yip, P. F., Moors, E. H., and Pardi, A. (1996) A network of heterogeneous hydrogen bonds in GNRA tetraloops, *J. Mol. Biol. 264*, 968−980.
4. Butcher, S. E., Dieckmann, T., and Feigon, J. (1997) Solution structure of a GAAA tetraloop receptor RNA, *EMBO J. 16*, 7490−7499.
5. Puglisi, E. V., and Puglisi, J. D. (1998) HIV-1 A-rich RNA loop mimics the tRNA anticodon structure, *Nat. Struct. Biol. 5*, 1033−1036.
6. Pley, H. W., Flaherty, K. M., and McKay, D. B. (1994) Three-dimensional structure of a hammerhead ribozyme, *Nature 372*, 68−74.
7. Fountain, M. A., Serra, M. J., Krugh, T. R., and Turner, D. H. (1996) Structural features of a six-nucleotide RNA hairpin loop found in ribosomal RNA, *Biochemistry 35*, 6539−6548.
8. Huang, S., Wang, Y. X., and Draper, D. E. (1996) Structure of a hexanucleotide RNA hairpin loop conserved in ribosomal RNAs, *J. Mol. Biol. 258*, 308−321.
9. Schweisguth, D. C., and Moore, P. B. (1997) On the conformation of the anticodon loops of initiator and elongator methionine tRNAs, *J. Mol. Biol. 267*, 505−519.
10. Durant, P. C., and Davis, D. R. (1999) Stabilization of the anticodon stem-loop of $tRNA^{Lys,3}$ by an A+C base-pair and by pseudouridine, *J. Mol. Biol. 285*, 115−131.
11. Cabello-Villegas, J., Winkler, M. E., and Nikonowicz, E. P. (2002) Solution conformations of unmodified and $A_{37}N^6$-dimethylallyl modified anticodon stem-loops of *Escherichia coli* tRNA(Phe), *J. Mol. Biol. 319*, 1015−1034.
12. Holbrook, S. R., Sussman, J. L., Warrant, R. W., Church, G. M., and Kim, S. H. (1977) RNA-ligand interactions:(I) magnesium binding sites in yeast $tRNA^{Phe}$, *Nucleic Acids Res. 4*, 2811−2820.
13. Quigley, G. J., Teeter, M. M., and Rich, A. (1978) Structural analysis of spermine and magnesium ion binding to yeast phenylalanine transfer RNA, *Proc. Natl. Acad. Sci. U.S.A. 75*, 64−68.
14. Shi, H., and Moore, P. (2000) The crystal structure of yeast phenylalanine tRNA at 1.93Å resolution: A classic structure revisited, *RNA 6*, 1091−1105.
15. Guéron, M., and Leroy, J. L. (1982) Significance and mechanism of divalent-ion binding to transfer RNA, *Biophys. J. 38*, 231−236.
16. Agris, P. F. (1996) The importance of being modified: roles of modified nucleosides and Mg^{2+} in RNA structure and function, *Progr. Nucleic Acid Res. 53*, 79−129.
17. Stuart, J. W., Gdaniec, Z., Guenther, R., Marszalek, M., Sochacka, E., Malkiewicz, A., and Agris, P. F. (2000) Functional anticodon architecture of human $tRNA^{Lys3}$ includes disruption of intraloop hydrogen bonding by the naturally occurring amino acid modification, t^6A, *Biochemistry 39*, 13396−13404.
18. Sundaram, M., Durant, P. C., and Davis, D. R. (2000) Hypermodified nucleosides in the anticodon of $tRNA^{Lys}$ stabilize a canonical U-turn structure, *Biochemistry 39*, 12575−12584.
19. Yue, D., Kintanar, A., and Horowitz, J. (1994) Nucleoside modifications stabilize Mg^{2+} binding in *Escherichia coli* $tRNA^{Val}$: an imino proton NMR investigation, *Biochemistry 33*, 8905−8911.
20. Leung, H. C., Chen, Y., and Winkler, M. E. (1997) Regulation of substrate recognition by the MiaA tRNA prenyltransferase modification enzyme of *Escherichia coli* K-12, *J. Biol. Chem. 272*, 13073−13083.
21. Davanloo, P., Rosenberg, A. H., Dunn, J. J., and Sturdier, F. W. (1984) Cloning and expression of the gene for bacteriophage T7 RNA polymerase, *Proc. Natl. Acad. Sci. U.S.A. 81*, 2035−2039.
22. Nikonowicz, E. P., Sirr, A., Legault, P., Jucker, F. M., Baer, L. M., and Pardi, A. (1992) Preparation of ^{13}C and ^{15}N Labeled RNAs for Heteronuclear Multi-Dimensional NMR Studies, *Nucleic Acids Res. 20*, 4507−4513.
23. Yamazaki, T., Muhandiram, R., and Kay, L. E. (1994) NMR experiments for the measurement of carbon relaxation properties in highly enriched, uniformly ^{13}C,^{15}N-labeled proteins: application to ^{13}C alpha carbons, *J. Am. Chem. Soc. 116*, 8266−8278.

24. Tewari, R. (1988) Conformational preferences of modified nucleic acid bases [N6-(Δ^2)-isopentenyl]-adenine and 2-methylthio-[N6-(Δ^2)-isopentenyl]-adenine by the quantum chemical PCILO calculations, *Int. J. Quantum Chem. 34*, 133−142.
25. Allain, F. H.-T., and Varani, G. (1995) Divalent metal ion binding to a conserved wobble pair defining the upstream site of cleavage of group I self-splicing introns, *Nucleic Acids Res. 23*, 341−350.
26. Gonzalez, R. L., and Tinoco, I. J. (2001) Identification and characterization of metal ion binding sites in RNA, *Methods Enzymol. 338*, 521−443.
27. Allain, F. H., and Varani, G. (1995) Structure of the P1 helix from group I self-splicing introns, *J. Mol. Biol. 250*, 333−353.
28. Kieft, J. S., and Tinoco, I. J. (1997) Solution structure of a metal-binding site in the major groove of RNA complexed with cobalt (III) hexammine, *Structure 5*, 713−721.
29. James, T. L., James, J. L., and Lapidot, A. (1981) Structural and dynamic information about double-stranded DNA from nitrogen-15 NMR spectroscopy, *J. Am. Chem. Soc. 103*, 6748−6750.
30. Nixon, P. L., Rangan, A., Kim, Y. G., Rich, A., Hoffman, D. W., Hennig, M., and Giedroc, D. P. (2002) Solution structure of a luteoviral P1−P2 frameshifting mRNA pseudoknot, *J. Mol. Biol. 322*, 621−633.
31. Majumdar, A., Kettani, A., Skripkin, E., and Patel, D. J. (2001) Pulse sequences for detection of NH2···N hydrogen bonds in sheared G·A mismatches via remote, nonexchangeable protons, *J. Biomol. NMR 19*, 103−113.
32. Poppe, L., and van Halbeek, H. (1994) NMR spectroscopy of hydroxyl protons in supercooled carbohydrates, *Nat. Struct. Biol. 1*, 215−216.
33. Conte, M. R., Conn, G. L., Brown, T., and Lane, A. N. (1996) Hydration of the RNA duplex r(CGCAAAUUUGCG)$_2$ determined by NMR, *Nucleic Acids Res. 24*, 3693−3699.
34. Gyi, J. I., Lane, A. N., Conn, G. L., and Brown, T. (1998) The orientation and dynamics of the C2′-OH and hydration of RNA and DNA·RNA hybrids, *Nucleic Acids Res. 26*, 3104−3110.
35. Hsu, S. T., Chou, M. T., and Cheng, J. W. (2000) The solution structure of [d(CGC)r(aaa)d(TTTGCG)]$_2$: hybrid junctions flanked by DNA duplexes, *Nucleic Acids Res. 28*, 1322−1331.
36. Nissen, P., Thirup, S., Kjeldgaard, M., and Nyborg, J. (1999) The crystal structure of Cys-tRNA^{Cys}-EF-Tu-GDPNP reveals general and specific features in the ternary complex in tRNA, *Structure 7*, 143−156.
37. Rüdisser, S., and Tinoco, I., Jr. (2000) Solution structure of cobalt-(III)hexammine complexed to the GAAA tetraloop, and metal-ion binding to G·A Mismatches, *J. Mol. Biol. 295*, 1211−1223.
38. Butcher, S. E., Allain, F. H.-T., and Feigon, J. (2000) Determination of metal ion binding sites within the hairpin ribozyme domains by NMR, *Biochemistry 39*, 2174−2182.
39. Hingerty, B. E., Brown, R. S., and Klug, A. (1982) Stabilization of the tertiary structure of yeast phenylalanine tRNA by [Co-(NH_3)$_6$]$^{3+}$. X-ray evidence for hydrogen bonding to pairs of guanine bases in the major groove, *Biochim. Biophys. Acta 697*, 78−82.
40. Striker, G., Labuda, D., and Vega-Martin, M. C. (1989) The three conformations of the anticodon loop of yeast tRNA^{Phe}, *J. Biomol. Struct. Dyn. 7*, 235−255.
41. Misra, V. K., and Draper, D. E. (2000) Mg^{2+} binding to tRNA revisited: the nonlinear Poisson−Boltzmann model, *J. Mol. Biol. 299*, 813−825.
42. Misra, V. K., and Draper, D. E. (1999) On the role of magnesium ions in RNA stability, *Biopolymers 48*, 113−135.
43. Gonzalez, R. L., and Tinoco, I. J. (1999) Solution structure and thermodynamics of a divalent metal ion binding site in an RNA pseudoknot, *J. Mol. Biol. 289*, 1267−1282.
44. Xu, Q., Jampani, S. R. B., and Braunlin, W. H. (1993) Rotational dynamics of hexaamminecobalt(III) bound to oligomeric DNA: correlation with cation-induced structural transitions, *Biochemistry 32*, 11754−11760.
45. Robinson, H., and Wang, A. H.-J. (1996) Neomycin, spermine and hexaamminecobalt(III) share common structural motifs in converting B- to A-DNA, *Nucleic Acids Res. 24*, 676−682.
46. Chen, Y., Sierzputowska-Gracz, H., Guenther, R., Everet, K., and Agris, P. F. (1993) 5-methylcytidine is required for cooperative binding of Mg^{2+} and a conformational transition at the anticodon stem-loop of yeast phenylalanyne tRNA, *Biochemistry 32*, 10249−10253.
47. Nobles, K. N., Yarian, C. S., Liu, G., Guenther, R. H., and Agris, P. F. (2002) Highly conserved modified nucleosides influence Mg^{2+}-dependent tRNA folding, *Nucleic Acids Res. 30*, 4751−4760.
48. Hall, K. B., Sampson, J. R., Uhlenbeck, O. C., and Redfield, A. G. (1989) Structure of an Unmodified tRNA molecule, *Biochemistry 28*, 5794−5801.
49. Ogle, J. M., Brodersen, D. E., Clemons, W. M. J., Tarry, M. J., Carter, A. P., and Ramakrishan, V. (2001) Recognition of cognate transfer RNA by the 30S ribosomal subunit, *Science 292*, 897−902.
50. Dix, D. B., Wittenberg, W. L., Uhlenbeck, O. C., and Thompson, R. C. (1986) Effect of replacing uridine 33 in yeast tRNAPhe on the reaction with ribosomes, *J. Biol. Chem. 261*, 10112−10118.
51. Ashraf, S. S., Ansari, G., Guenther, R., Sochacka, E., Malkiewicz, A., and Agris, P. F. (1999) The uridine in "U-turn": contributions to tRNA-ribosomal binding, *RNA 5*, 503−511.
52. Davis, D. R., and Poulter, C. D. (1991) ^{1}H-^{15}N NMR studies of *Escherichia coli* tRNA^{Phe} from hisT mutants: a structural role for pseudouridine, *Biochemistry 30*, 4223−4231.
53. Houssier, C., and Grosjean, H. (1985) Temperature jump relaxation studies on the interactions between transfer RNAs with complementary anticodons. The effect of modified bases adjacent to the anticodon triplet, *J. Biomol. Struct. Dyn. 3*, 387−408.
54. Turnbough, C. L., Jr., Neill, R. J., Landsberg, R., and Ames, B. N. (1979) Pseudouridylation of tRNAs and its role in regulation in *Salmonella typhimurium*, *J. Biol. Chem. 254*, 5111−5119.
55. Raychaudhuri, S., Niu, L., Conrad, J., Lane, B. G., and Ofengand, J. (1999) Functional effect of deletion and mutation of the *Escherichia coli* ribosomal RNA and tRNA pseudouridine synthase RluA, *J. Biol. Chem. 274*, 18880−18886.
56. Esberg, B., Leung, H. C., Tsui, H. C., Bjork, G. R., and Winkler, M. E. (1999) Identification of the miaB gene, involved in methylthiolation of isopentenylated A37 derivatives in the tRNA of *Salmonella typhimurium* and *Escherichia coli*, *J. Bacteriol. 181*, 7256−7265.
57. Newby, M. I., and Greenbaum, N. L. (2002) Sculpting of the spliceosomal branch site recognition motif by a conserved pseudouridine, *Nat. Struct. Biol. 9*, 958−965.

BI0353676